WATER RESOURCES RESEARCH, VOL. 37, NO. 12, PAGES 2981–2994, DECEMBER 2001

Simulations of two-dimensional modeling of biomass aggregate growth in network models

Hubert J. Dupin,[1] Peter K. Kitanidis, and Perry L. McCarty

Department of Civil and Environmental Engineering, Stanford University, Stanford, California, USA

Abstract. We investigate the mechanisms by which microorganism that grow in the form of aggregates impact the permeability and the transport properties of porous media modeled as two-dimensional networks. In a companion paper [*Dupin et al*., this issue] we present a model of processes in a single channel. In this paper, we describe how to assemble channels into networks. Simple networks are investigated to identify phenomena of interest: four channels of different width operating in parallel to study the effect of local heterogeneity; a periodic network to quantify the effects of distance from the injection point on clogging and substrate utilization; and square lattice 5×5 random width networks. Although square lattice random width networks are deemed better approximations of porous media, the simpler networks exhibit all the phenomena of interest, with the added advantage of these phenomena being decoupled. Results of numerical simulations for different network types under various boundary conditions show that aggregates have a far greater potential than biofilms to clog a porous medium.

1. Introduction

Among the many different technologies that are available to clean up a polluted site, in situ bioremediation is one of the most promising [*Miller et al*., 1991]. From an engineering perspective, in situ bioremediation has many similarities with biofiltration in the sense that microorganisms grow in porous media utilizing substrate and nutrients, which are often provided by forcing a feed solution through the system. Clogging may affect the operation and the cost of an in situ bioremediation project [*McCarty et al*., 1998]. Given that experimental data on clogging appear sparingly in the literature, it seems reasonable to apply models developed for water treatment units to bioremediation. Many of the models [*Chen et al*., 1994; *Clement et al*., 1996; *Suchomel et al*., 1998a, 1998b; *Taylor and Jaffe*, 1990b, 1991; *Wanner et al*., 1995] assume that soil grains are uniformly covered by microorganisms, i.e., a biofilm, as this is the primary form of growth observed in biofilters for wastewater treatment. *Rittmann* [1993] indicated that a continuous biofilm can be sustained with high loadings and that only microcolonies tend to develop under low loadings. Models have also been developed assuming a patchy biofilm [*Molz et al*., 1986; *Widdowson*, 1991].

However, *Rittmann* [1993] and *Vandevivere et al*. [1995] have indicated that the biofilm model underestimates permeability reduction and that models that consider the presence of aggregates are likely to predict clogging more accurately in finely grained porous media. Colony morphologies in porous media can be diverse and concurrent [*Dupin and McCarty*, 2000]; that is, one may observe a biofilm and microcolonies, as well as aggregates [*Dupin and McCarty*, 2000; *Vandevivere and Baveye*, 1992b], biowebs [*Dupin and McCarty*, 2000; *Paulsen et al*., 1997], and filamentous fungi [*Dupin and McCarty*, 1999], whose effects on clogging have not been modeled as yet.

Network models of porous media consist of interconnected channels with different network topologies [*Berkowitz and Ewing*, 1998; *Koplik*, 1981]. Networks are commonly used in earth sciences as models for numerical simulations [*Blunt*, 1997; *Fatt*, 1956a, 1956b, 1956c; *Suchomel et al*., 1998a, 1998b]. They are also used in laboratory experiments [*Dupin and McCarty*, 1999; *Laroche-Jaffrennou et al*., 1999] because they allow partial modeling of flow patterns down to the pore level, which is not achievable with soil cores.

The approach followed in this work is to simulate the effect of aggregate growth on substrate transport and permeability in different network topologies. Several simple networks are used in order to gain a basic understanding of the mechanisms that control the growth and distribution of biomass. The modeling approximations and the numerical implementation at the scale of a single channel have been detailed previously [*Dupin et al*., this issue; *Dupin*, 1999]. In summary, each channel in the network is seeded with initial biomass that requires for survival and growth an electron donor and an electron acceptor according to dual Monod kinetics (Figure 1). The Stokes flow, advection-diffusion-reaction, and biomass deformation partial differential equations are solved using finite elements. Biomass is modeled as a continuous uniform isotropic hyperelastic material, whose expansion and deformation are governed by material mechanics stress-strain relations.

This paper will describe how the pore network model is defined and operated and will present results of numerical simulations. Three types of boundary conditions are considered to apply on the network:

1. In the fixed-head boundary condition the head difference across the network $\Delta\varphi$ is kept constant. As clogging occurs, the total flow Q through the network decreases, simulating conditions that might occur under natural attenuation.

2. In the fixed-flow boundary condition a constant flow rate is enforced through the network. This might simulate condi-

[1]Now at Geosciences Department, Exploration-Production Division, Gaz de France, Saint-Denis-La-Plaine, France.

Paper number 2001WR000310.
0043-1397/01/2001WR000310$09.00

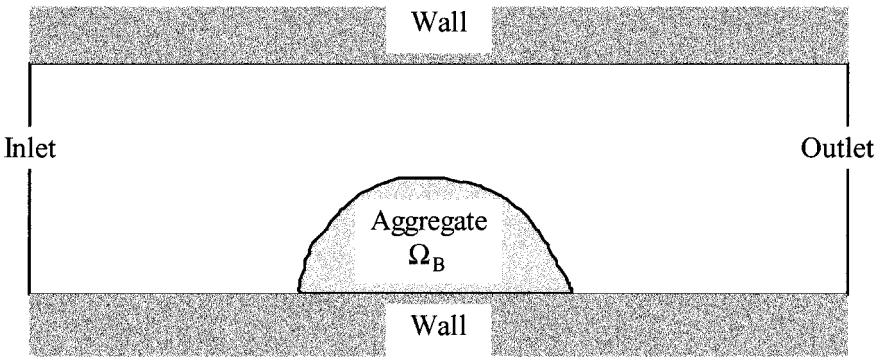

Figure 1. Schematic drawing of a channel.

tions prevalent during enhanced bioremediation, when nutrients are pumped at a fixed-flow rate into the aquifer.

3. In the fixed-power boundary condition the product $\Delta\varphi \cdot Q$ is kept constant. As the head builds up, the total flow pumped into the aquifer decreases.

2. Network Model

In the network model one must simulate processes in each channel and node as well as the interactions between adjacent channels and nodes. In particular, one must describe the head loss, the transport of solutes, and the substrate consumption in every channel and node. Figure 2 shows channel interactions at a generic node i. Numerically, channels are simulated individually using computer programs to be called "channels." Coordination is achieved through another computer program called the "network driver" that provides these channels with boundary conditions (head values and concentration values), essentially enforcing consistency of boundary conditions at the nodes. Channels return information to the driver (permeability, substrate consumption, and shape of the aggregates). Figure 3 shows the general architecture of the network model. The network driver defines the network structure: channel dimensions, connectivity of nodes and channels, and location of injection and withdrawal points.

2.1. Head Loss

2.1.1. Network model description. Let φ_i be the head at node i. We assume that all head loss takes place within channels, neglecting the small head loss in nodes. Let nodes i and j be connected through a channel, let q_{ij} be the flux from node i to node j, and let k_{ij} be the conductance associated with channel i-j. Evaluation of conductance k_{ij} has been discussed elsewhere [*Dupin et al.*, this issue], because it depends on the shape of the aggregates within the channel. Note that $k_{ji} = k_{ij}$ and $q_{ij} = -q_{ji}$. If two nodes i and j are not connected directly by a channel, $k_{ij} = 0$. From Darcy's law, we obtain

$$q_{ij} = k_{ij}(\varphi_i - \varphi_j). \tag{1}$$

At each node i within the system, conservation of mass implies

$$\sum_j q_{ij} = 0 = \sum_j k_{ij}(\varphi_i - \varphi_j), \tag{2}$$

while at the injection node ($i = 1$),

$$\sum_j q_{1j} = Q_{\text{total}} \tag{3}$$

and at the withdrawal node ($i = n$)

$$\sum_j q_{nj} = -Q_{\text{total}}. \tag{4}$$

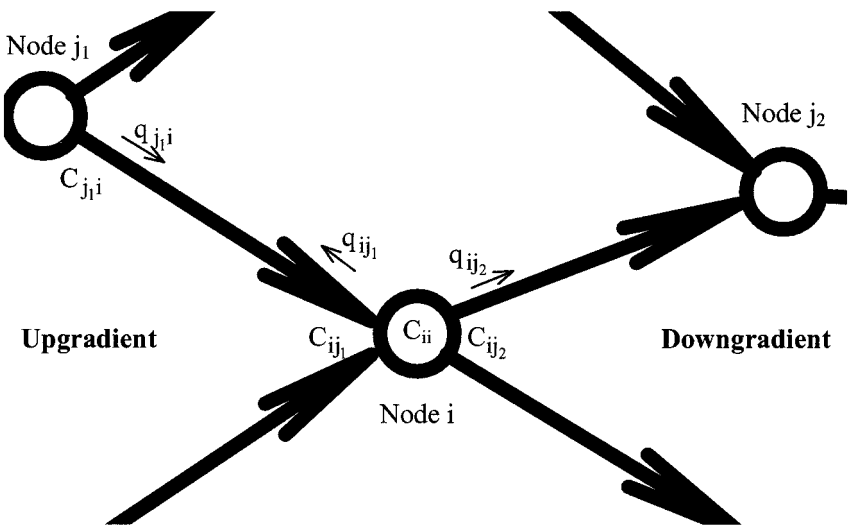

Figure 2. Channel interactions at a generic node i.

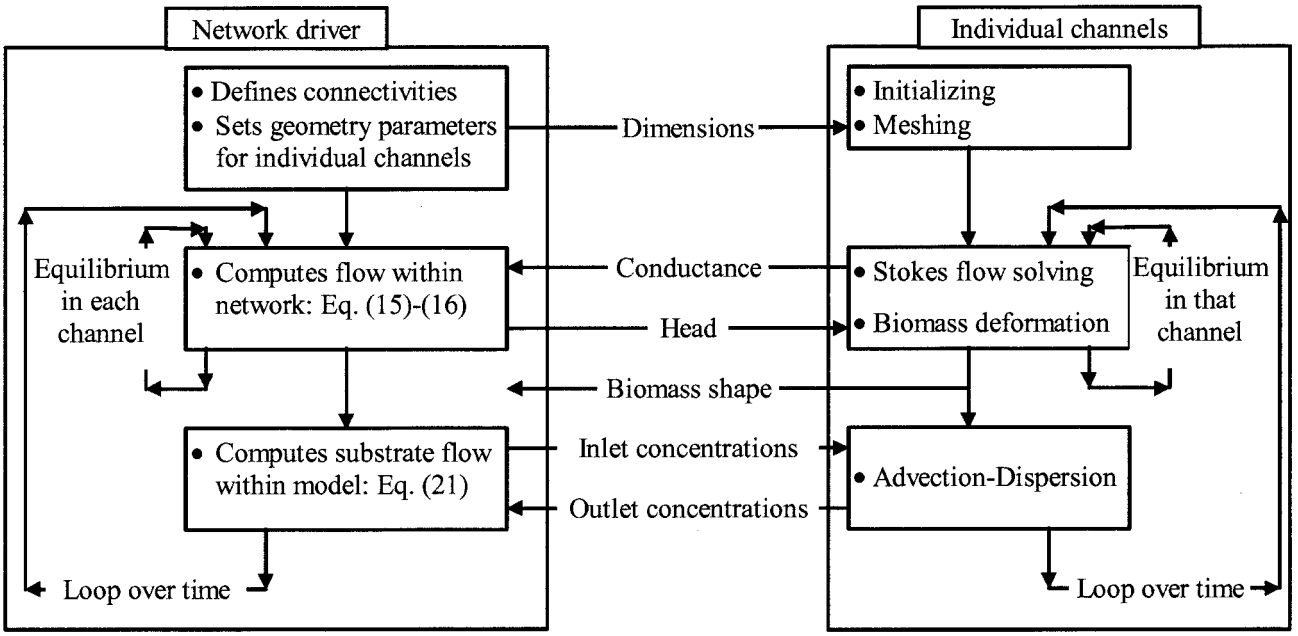

Figure 3. Architecture of the network model.

The total head loss across the system is

$$\varphi_1 - \varphi_n = Q_{\text{total}}/K, \tag{5}$$

where K is the conductance of the whole network; it is equal to the discharge for unit head difference $\varphi_1 - \varphi_n$.

Next, define the symmetric matrix $[K]$ as

$$K_{ij} = -k_{ij} \qquad i \neq j \tag{6}$$

$$K_{ii} = \sum_j k_{ij}. \tag{7}$$

We can rewrite (1)–(4) as

$$[K](\Phi) = (Q), \tag{8}$$

defining the vectors $(\Phi) = (\varphi_i)$ and $(Q) = \begin{pmatrix} Q_{\text{total}} \\ 0 \\ \vdots \\ 0 \\ -Q_{\text{total}} \end{pmatrix}$.

Matrix [**K**] is singular. Indeed, if (Φ) is a solution, $(\Phi) + \varphi_0$ is also solution for any φ_0. Without loss of generality, because flow is affected by head differences only, we can assume

$$\varphi_n = 0 \tag{9}$$

and substitute this equation for (4). Substituting φ_n by 0 in (2), we can formally suppress k_{in} in (2), modifying the last column of $[K]$. Matrix $[K]$ can be replaced by

$$[K'] = \begin{bmatrix} & & 0 \\ [K_{i,j}]_{1\le i,j\le n-1,} & & \vdots \\ & & 0 \\ 0 & \cdots 0 & 1 \end{bmatrix}, \tag{10}$$

and (Q) can be replaced by (Q') as

$$(Q') = \begin{pmatrix} Q_{\text{total}} \\ 0 \\ \vdots \\ 0 \end{pmatrix}. \tag{11}$$

Because we may not know Q_{total}, we will seek a solution (Φ'') for a unit head difference, that is,

$$\varphi_1 = 1. \tag{12}$$

Similarly to (9)–(11), φ_1 is substituted by 1, leading to further modification of $[K']$ into

$$[K''] = \begin{bmatrix} 1 & 0 \cdots 0 & 0 \\ 0 & & \vdots \\ \vdots & [K_{i,j}]_{2\le i,j\le n-1} & \\ 0 & & 0 \\ 0 & 0 \cdots 0 & 1 \end{bmatrix} \tag{13}$$

and (Q') into

$$(Q'') = \begin{pmatrix} 1 \\ (k_{1i})_{2\le i\le n-1} \\ 0 \end{pmatrix}; \tag{14}$$

$[K'']$ is positive definite [*Suchomel et al.*, 1998b]. Thus we solve

$$[K''](\Phi'') = (Q''). \tag{15}$$

If the head difference is prescribed, the solution (Φ'') must be multiplied by the head difference. If the total discharge is specified, the solution (Φ'') must be adjusted by multiplying it with a coefficient equal to the ratio of Q_{total} to the discharge obtained for unit head difference, i.e.,

$$(\Phi) = \frac{Q_{\text{total}}}{\sum_{1\le j\le n} K_{1,j}\Phi''_j}(\Phi''). \tag{16}$$

The total power P needed to force flow through the network balances the losses through all the individual channels:

$$P = \frac{1}{2} \sum_{i,j} q_{ij}(\varphi_i - \varphi_j) = \frac{1}{2} \sum_{i,j} k_{ij}(\varphi_i - \varphi_j)(\varphi_i - \varphi_j). \quad (17)$$

The coefficient 1/2 compensates for the double accounting of each channel. Developing (17) and recalling the definition of K_{ij},

$$P = \frac{1}{2}\left[\sum_i \left(\sum_j k_{ij} \right) \varphi_i^2 + \sum_j \left(\sum_i k_{ij} \right) \varphi_j^2 - 2 \sum_{i \neq j} k_{ij}\varphi_i\varphi_j \right]$$

$$P = \sum_i K_{ii}\varphi_i^2 + \sum_{i \neq j} K_{ij}\varphi_i\varphi_j, \quad (18)$$

and finally

$$P = (\Phi)^T[K](\Phi) = Q_{\text{total}}(\varphi_1 - \varphi_n) = (\Phi)^T(Q). \quad (19)$$

However, there is no unique (Φ) verifying (19) as explained above.

Because growth is much slower than substrate transport and flow equilibration, biomass is assumed not to expand in size for a certain time interval Δt but, instead, to slightly increase in density. This Δt value is chosen so that the temporary density increase is less than 5% of the average density. Thus conductance and average velocity in each channel remain constant during Δt, and the flow problem is decoupled from substrate transport and biomass growth.

2.1.2. Network driver operation. All the channels compute their conductances simultaneously, assuming that each is subject to a certain head difference, and return these values to the network driver (Figure 3). Once all the channels have provided conductance values, the network driver solves (15) and (16) and returns to each channel its head drop. These head values might be different from those assumed by the channels to initiate conductance computations.

To reduce the computational cost, the aggregates are not allowed to deform because of flow forces. Otherwise, a different head across a channel would lead to both different flow velocities within that channel and different forces on its aggregate than those initially assumed. Aggregates would then take another shape, and channel conductance would be modified. The channels would then return a new conductance to the network driver, which would again solve (15) and (16). These nested fluid-structure interactions, at the channel level and at the network level, are likely to result in lengthy computations, deemed unnecessary for this work.

2.2. Substrate Reactive Transport

2.2.1. Network model description. We assume complete mixing and conservation of substrate mass at the nodes of the network. Diffusion from a node back into the channels discharging into it is neglected, as discussed in section 2.2.3.

Let C_{ij} be the concentration of electron acceptor (oxygen) or electron donor (phenol) in the channel between node i and j, next to the node i; C_{ji} is the concentration at the other end. Let C_{ii} be the concentration at node i resulting from mixing (Figure 2). Let j_1 be a generic index for the upgradient nodes j connected to the node i (thus $q_{ij_1} < 0$), and let j_2 be a generic index for the downgradient nodes j connected to node $i (q_{ij_2} > 0)$. Our hypothesis states that the incoming fluxes at concentrations C_{ij_1} get perfectly mixed, and the concentration of the outgoing fluxes C_{ij_2} equal the mixing concentration C_{ii}:

$$C_{ij_2} = C_{ii} = \frac{\sum_{j_1} q_{ij_1} C_{ij_1}}{\sum_{j_1} q_{ij_1}}, \quad (20)$$

where $q_{ij_1} < 0$ and $q_{ij_2} > 0$.

In general, $C_{ij_2} \neq C_{j_2 i}$, because of transformation in the biomass within the channel from i to j_2. Substrate consumption is computed as described by *Dupin et al.* [this issue].

2.2.2. Network driver operation. After solving the network flow problem, the network driver sends to the channels directly connected to the injection node their influent concentration C_{1j_2}. They compute the substrate transport problem and return an effluent concentration (Figure 3).

Once all the concentrations C_{ij_1} of the channels discharging into node i are known, the driver computes the mixing concentration C_{ii} by (20) and sends C_{ij_2} to all the downgradient channels directly connected to that node i. Eventually, all the nodal concentrations are known one after the other, the last one being that of the withdrawal node. To simplify the passing of parameters between the channels and the network driver, this process has been modified as follows. Instead of passing the instantaneous influent and effluent concentrations, we average over a short period Δt the effluent concentrations of the channels before communicating these concentrations to the network driver. Similarly, the influent concentration of the downgradient channel is constant during that same period Δt. This Δt value is chosen as the time period during which biomass is considered not to expand but to increase in density, and channel fluid velocities are constant. Thus (20) becomes

$$\forall\, t \in [t_1, t_1 + \Delta t[, \qquad \forall\, j_2 | q_{ij_2} > 0,$$

$$C_{ij_2}(t) = C_{ii}(t) = \frac{\sum_{j_1 | q_{ij_1} < 0} q_{ij_1}(t_1) \int_{t_1}^{t_1 + \Delta t} C_{ij_1}(t)\, dt}{\Delta t \sum_{j_1 | q_{ij_1} < 0} q_{ij_1}(t_1)}. \quad (21)$$

If Δt is sufficiently short, (20) is equivalent to (21). Halving this Δt value showed no significant difference in values of concentration or conductance in numerical tests.

This network scheme to compute concentrations is both sequential and parallel. It is sequential in the sense that all the upgradient channels $j_1 - i$ of a specific node i must be known before computations can start in any downgradient channel $i - j_2$. However, it is also a parallel process in the sense that computations in all the channels $i - j_2$ can be simultaneously evaluated. Thus one may save time by performing computations in parallel on several computers.

2.2.3. Channel boundary conditions. The boundary conditions of the individual channels are given by the following equations [*Dupin et al.*, this issue], x axis being in the main flow direction (with $x = 0$ at the center of the aggregate):

Constant supply on inlet

$$u_{\text{ave}} C - D \frac{\partial C}{\partial x} = u_{\text{ave}} C_{\text{supply}}, \quad (22)$$

No diffuse flux at outlet

$$\frac{\partial C}{\partial x} = 0, \quad (23)$$

No flux through the wall

$$\frac{\partial C}{\partial y} = 0. \tag{24}$$

At $t = 0$, $C = C_{\text{supply}}$ for the electron donor and the electron acceptor throughout the entire channel.

Let Pe_d be $(u_{\text{ave}}d)/D$, where d is the distance from the channel inlet boundary to the aggregate and D is the dispersion coefficient. Away from the aggregate, substrate is subject to one-dimensional (1-D) advection and diffusion. Isoconcentration lines are perpendicular to the main channel axis, and concentration gradients change exponentially with distance from the inlet (as in a 1-D channel subject to steady state advection and dispersion with no sink). Such an advection-dispersion problem is described by

$$D\,\frac{\partial^2 C}{\partial x^2} = u_{\text{ave}}\,\frac{\partial C}{\partial x}, \tag{25}$$

where D is the dispersion coefficient. The solution to this differential equation subject to the condition that the inlet flux is $u_{\text{ave}}C_{\text{supply}}$, i.e., consistent with (22), for $x < 0$ is

$$C(x) = C_{\text{supply}}(1 - \alpha \exp(u_{\text{ave}}x/D)), \tag{26}$$

where α depends on the substrate consumption in the biomass. At the inlet the solution of this differential equation can be written ($d = -x$, thus $d > 0$):

$$C_{\text{inlet}} = C_{\text{supply}}(1 - \alpha e^{-Pe_d}). \tag{27}$$

$Pe_d = 1$ corresponds to $u_{\text{ave}} = 70$ cm d^{-1} based on a diffusional distance of 300 μm and a dispersion coefficient equal to the aqueous diffusion coefficient of oxygen ($\sim$2 cm^2 d^{-1}). Because channels are sufficiently long and the average velocities that we consider are sufficiently high, $Pe_d \gg 1$ in most cases, which means that there is practically no discontinuity in the concentration at the node-channel interface. Here the substrate influent concentration C_{supply} is communicated by the network driver, that is, $C_{\text{supply}} = C_{ii} = C_{ij_2}$; see (21).

Downgradient of the aggregate, substrate concentration obeys a similar 1-D solution:

$$C(x) = C_1 + C_2 \exp(u_{\text{ave}}x/D). \tag{28}$$

The flux discharged at the outlet of the channel is $u_{\text{ave}}C_1$, independent of C_2, which is arbitrarily set to 0 in (23). Because C is bounded (between 0 and the network influent concentration), when $Pe_d \gg 1$, we have $C_2 \ll 1$. Thus close to the aggregate, but sufficiently far so that (28) applies, (23) is almost satisfied as we there have $C_2 \exp(u_{\text{ave}}x/D) \ll 1$. That is, (23) does not have an impact on the channel results, in terms of substrate consumption or flux of substrate discharged. Keeping (23), we have $C_{\text{outlet}} = C_1$. However, (23) may give different results for the actual concentration at the outlet as explained below.

Figure 4 illustrates (20), (22), and (27) when Pe_d is not very large and (23) is relaxed. Two channels $1 - i$ and $2 - i$ at concentrations C_{i1} and C_{i2} merge into node i. The mixing concentration C_{ii} is displayed by the dotted line. Downgradient, two channels $i - 3$ and $i - 4$ emanate from node i with concentrations C_{i3} and C_{i4}, respectively, that are lower than the mixing concentration of the node $C_{\text{supply}} = C_{ii}$. The total flux of substrate at any downgradient node-channel interface ($i - 3$ or $i - 4$) is $u_{\text{ave}}C_{\text{supply}}$. Physically, concentration is continuous. Thus, in reality, the concentration at the channel inlet would increase to match the concentration in the node, which, in turn, would go down. Similarly, the concentrations at the upgradient channel outlets go down (as shown), leading to a gradient that vanishes when going farther upgradient within these channels; if $Pe_d \gg 1$ is not satisfied within the upgradient channel, this gradient would still be felt close to the aggregate, and this would create a "pull" on the concentration farther upgradient. However, owing to the particular network configurations we select, the nodal concentration drop would be insignificant as the flow through a narrow clogged channel is negligible compared to the total flow through a node in our network. When $Pe_d \gg 1$ is not satisfied, we underestimate substrate flux, nutrient aggregate uptake, and aggregate growth in a clogged channel. Indeed, recalling (27), $C_{\text{inlet}} = C_{\text{node}}$ leads to $C_{\text{supply}} > C_{\text{node}}$; that is, a clogged channel actually receives more substrate than we predict through (20). In this case all the channels of the network are tightly coupled, and the network needs to be solved as a whole.

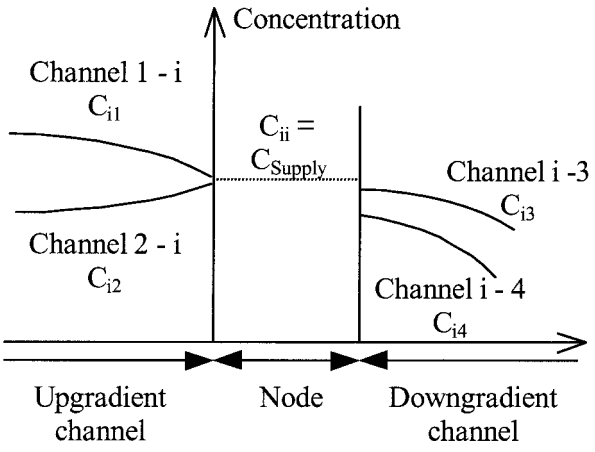

Figure 4. Schematic of concentration values around the node-channel interfaces illustrating the boundary conditions.

3. Results

We have used three network types: a simple network consisting of four channels of different widths operating in parallel, a periodic network, and square lattice 5×5 random width networks.

The channel model and the network driver have been written using Matlab 5.1 for Sun WorkStation (see The MathWorks Inc. at www.mathworks.com), using Matlab routines for meshing and solving linear systems of equations. The communication routines between the individual channels and the network driver have been written in Tcl 7.8 (see Sun Microsystems Laboratories at www.scriptics.com). Table 1 lists the values of the model parameters.

3.1. Four Channels in Parallel

The four channels are 50, 100, 150, and 200 μm wide and 600 μm long. The goal of this computational experiment is to estimate the effect of local heterogeneity on clogging, biomass growth, and substrate transport. Because they operate in par-

Table 1. Model Parameters[a]

Parameter	Value	Signification
Dimensions	600 μm	channel length
	typically 100 μm[b]	channel width
	5 μm	size of the initial seed
Temperature	20°C	
Biological kinetics		
K_{sA}	1.0 mg L^{-1}	saturation constant for oxygen
K_{sD}	1.0 mg L^{-1}	saturation constant for phenol
k	9.3 mg mg^{-1} d^{-1}	maximum utilization rate
Y	0.61 mg mg^{-1}	yield coefficient
b	0.12 day^{-1}	decay coefficient
f_d	0.8 mg mg^{-1}	degradable biomass fraction
d_c	1.42 mg mg^{-1}	decay oxygen demand
COD	2.38 mg mg^{-1}	chemical oxygen demand of phenol
$F = \text{COD} - Yd_c$	1.52 mg mg^{-1}	oxygen to phenol utilization ratio
X_m	30,000 mg L^{-1}	maximum solids concentration in aggregate
$X_{a\ \text{start}}$	$X_m 1$	initial active biomass concentration ($f_a = 1$)
Hydrodynamics		
D_a	2.32 cm^2 d^{-1}	aqueous oxygen diffusion
D_{fa}	1.85 cm^2 d^{-1}	oxygen diffusion coefficient in aggregate
D_d	1.01 cm^2 d^{-1}	aqueous phenol diffusion
D_{fd}	0.81 cm^2 d^{-1}	phenol diffusion coefficient in aggregate
g	9.81 m s^{-2}	gravity
ρ	998 mg cm^{-3}	density of water
υ	0.01003 cm^2 s^{-1}	kinematic viscosity of water
λ	2.10^3	relative viscosity of water in aggregate
Iterations		
Δt	12 min	time step to update shape of biomass

[a]Table units are milligrams, centimeters, and days.
[b]See text.

allel, the four channels are subject to the same head. They are all seeded with the same amount of biomass.

The "base case" consists in applying a starting head across the network of 10^{-5} m, which would eventually increase under fixed-power and fixed-flow conditions as the network clogged. Thus the initial average velocities are 2.9, 12, 27, and 47 m d^{-1} in the 50, 100, 150, and 200 μm wide channels, respectively, resulting in the initial average velocity across the whole network being 30 m d^{-1}. These high velocities are representative of conditions close to an injection well. The initial hydraulic conductivities are 2×10^{-3}, 8.2×10^{-3}, 1.8×10^{-2}, and 3.2×10^{-2} m s^{-1} for the channels and 2×10^{-2} m s^{-1} for the network. Accounting for solid space the overall conductivity would be less. For example, for a porous medium with porosity 0.35, the average conductivity would be 0.7×10^{-2} m s^{-1}, which corresponds to coarse sand or fine gravel.

Fixed-head, fixed-power, and fixed-flow conditions lead to different responses of the system. In all our simulations, clogging occurs within 2 days, in part because of the cell doubling time of ~3 hours.

The network hydraulic conductivity follows closely that of the wider channels. The narrowest pores clog first (Figure 5), but the network conductivity does not drop appreciably until the widest pores clog. In other words, fixed-head, fixed-power, or fixed-flow conditions lead initially to very similar network behaviors until the narrowest channel is clogged. For example, under fixed-flow conditions the head across the network equals 1.06×10^{-5} m when the conductivity of the narrower channel is halved, very close to its initial head of 1×10^{-5} m.

Figure 6 shows the channel effluent concentration as a function of time under fixed-head conditions. Because of the stoechiometry, phenol is in excess as the system is fed phenol and

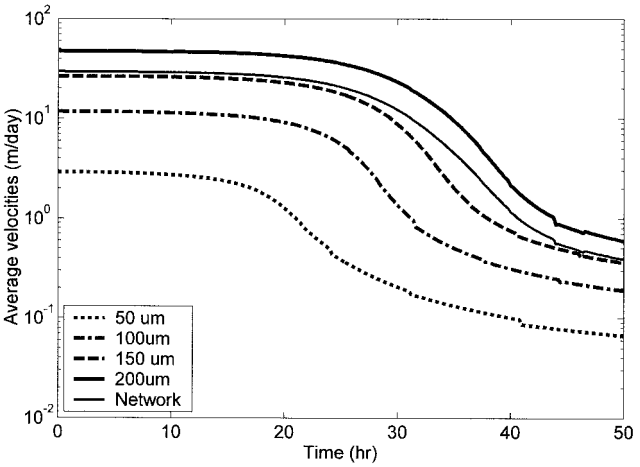

Figure 5. Average velocities as a function of time in four parallel channels under a fixed head of 10^{-5} m. Average velocities are proportional to the hydraulic conductivities under fixed-head condition.

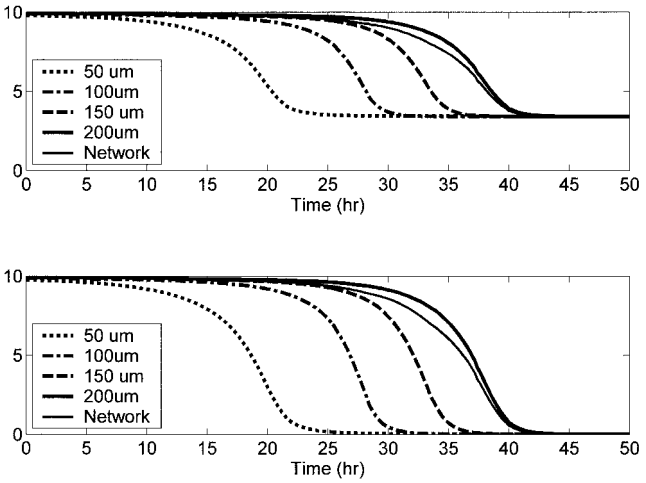

Figure 6. Effluent concentration as a function of time of four parallel channels under a fixed head of 10^{-5} m: (top) electron donor concentration at outlet, C_D/K_{sD}, and (bottom) electron acceptor concentration at outlet, C_A/K_{sA}.

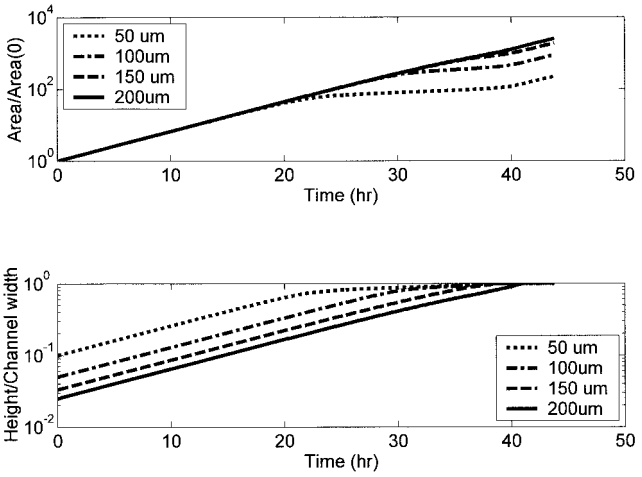

Figure 8. Aggregate growth as a function of time in four parallel channels with an average discharge across the network of 30 m d^{-1}: (top) relative area (with respect to start) versus time and (bottom) relative height (with respect to channel width) versus time.

oxygen at the same concentration $10K_S$, meaning that when oxygen is exhausted, phenol concentration is $3.4K_S$. The effluent electron acceptor concentration decreases faster for the narrowest channels than for the widest channels, and the effluent electron acceptor concentration of the network is strongly correlated to that of the widest channel. Until a channel clogs, its aggregate grows exponentially with an average growth rate of 4.5 day^{-1}, slightly less than the maximum growth rate of $[kY\,C_D/(C_D + K_{S_D}) - b][C_A/(C_A + K_{S_A})] = 4.6$ day^{-1}, obtained by substituting C_A and C_D with the supply values $10K_S$. This indicates that the aggregates are fully penetrated and that diffusional resistance does not slow growth. When a channel clogs, its effluent concentration drops, and its aggregate growth rate decreases to 0.23 day^{-1}.

Under preset flow conditions the four channels are coupled: The total flux through the network is fixed, and total flux partitions between the channels (Figure 7). As long as the widest channel is not clogged, velocities in the narrowest channels decrease, similarly to the fixed-head case. However, when the widest channel clogs, the narrowest channels become relatively more permeable, and flow is rerouted through them. Indeed, at $t = 42$ hours the average velocity in the narrowest channel is 16 times higher than at $t = 37$ hours and 2.8 times higher than at $t = 0$. As a result of flow recovery, growth resumes in the narrowest channels. Figure 8 shows the aggregate areas and heights as a function of time. One can observe the initial exponential growth with a growth rate of 4.5 day^{-1}, followed by slowing to a growth rate of 0.72 day^{-1} when channels clog, and upsurging again to a rate of 4.15 day^{-1} in channels when flow is rerouted. This rapid growth indicates a breakthrough of concentration (Figure 9). For the fixed-flow conditions, computations were stopped because the aggregates overflowed from the channels.

The "plateau" growth rate of 0.72 day^{-1} under fixed-flow conditions is higher than 0.23 day^{-1} obtained under fixed-head

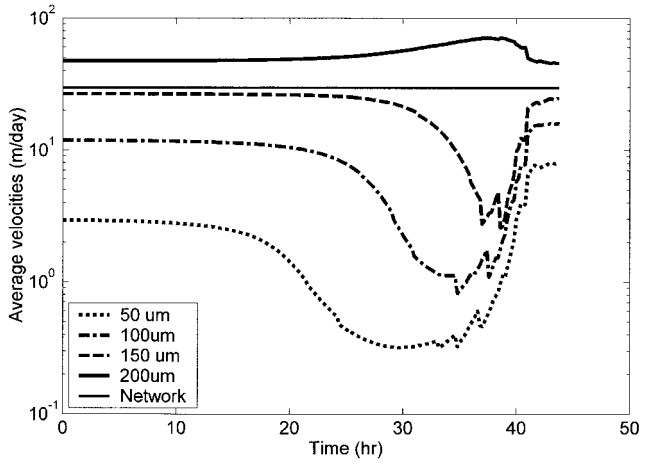

Figure 7. Average velocity as a function of time under fixed flow in four parallel channels with an average discharge across the network of 30 m d^{-1}.

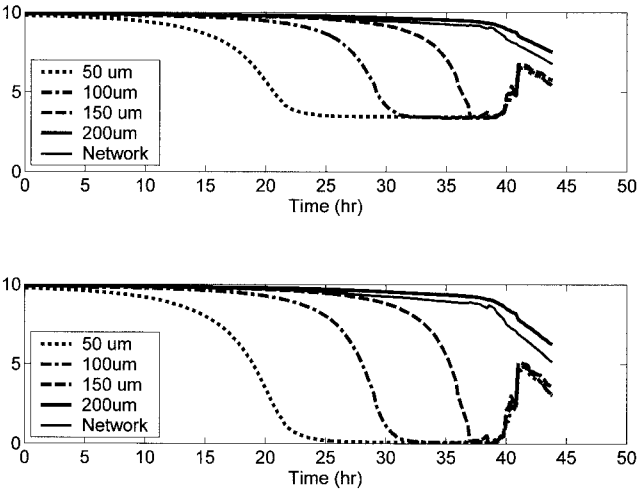

Figure 9. Effluent concentration as a function of time of four parallel channels with an average discharge across the network of 30 m d^{-1}: (top) electron donor concentration at outlet, C_D/K_{sD}, and (bottom) electron acceptor concentration at outlet, C_A/K_{sA}.

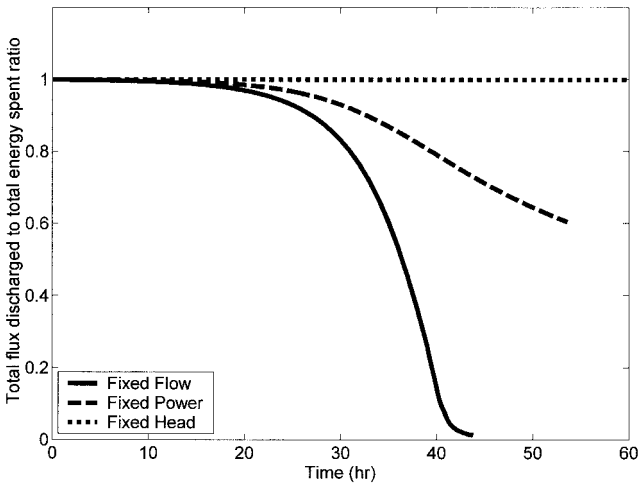

Figure 10. Efficiency as defined by the ratio $\int_0^t Q\ dt/[\int_0^t Q(\Delta\varphi/\Delta\varphi_{t=0})\ dt]$ of different pumping schemes with identical starting conditions.

conditions. The reason is simple: Flow through the network is not reduced, unlike under fixed-head conditions, and thus more substrate is fed into the channels, and more biomass can grow on it.

Characteristic times for the electron acceptor channel effluent concentration (i.e., time when outlet concentration is halved) vary between 19 and 37 hours under fixed-head conditions for the base case. Those characteristic times are longer by 0.2–1.6 hours under operating conditions that result in higher fluid velocities through the network: fixed-flow or fixed-power conditions; doubling the flow, power, or head; or halving the water pseudoviscosity in the aggregate. Because conductivities tend to decrease over time, the ratio $\int_0^t Q\ dt/[\int_0^t Q(\Delta\varphi/\Delta\varphi_{t=0})\ dt]$ of the total volume since the beginning of the treatment to the total pumping energy tends to decrease (Figure 10). The head is normalized to the initial head difference. This ratio is a useful measure of the relative effectiveness of pumping in forcing the flow through the network, that is, the relative effectiveness of supplying substrate to the network. It is 1 for the fixed-head scenario. It takes its lowest values for fixed-flow conditions because, while Q = const, the normalized head $\Delta\varphi/\Delta\varphi_{t=0}$ increases dramatically as the system gradually becomes clogged. This measure (Figure 10) shows how much more energy it takes to run a system in the constant flow mode compared to the constant head one. The ratio decreases much less for the fixed-energy case, because as the head difference increases, the flow rate decreases thus slowing down the rate of clogging.

Table 2 lists the conductivity decrease factors for each channel for the three operating conditions. Conductivity decreases the most under fixed flow and the least under fixed head, as expected. Under fixed flow, substrate is forced into the aggregate, which thus keep on expanding. Under fixed head, substrate supply occurs mainly slowly by diffusion once the flow in the clogged channels is diminished.

Table 2 also demonstrates that conductivity decreases by larger factors in the wider channels than in the narrower ones. The range of velocities, represented by the ratio of the average velocity in the widest pore to that in the narrowest pore, is ultimately reduced. The larger the range is, the greater are the macrodispersive effects. At early times, as we have seen, the

Table 2. Ratio of Initial Conductivities to Final Conductivities for Different Boundary Conditions

	Fixed Head	Fixed Power	Fixed Flow
50 μm	44	230	490
100 μm	62	400	1010
150 μm	74	600	1460
200 μm	80	780	1410
Network	75	660	1360
Final Time, hours	50	50	43.8[a]

[a]Simulations are stopped after 43.8 hours for the fixed-flow scheme because aggregates overflow from the channels.

opposite may happen: The narrowest channel clogs, while the widest channel is still unaffected. Thus there is a temporary increase in the dispersion span. Table 3 shows the extent of the span under different operating conditions. While the initial span is 16, it is reduced by a factor 2–3 after clogging but can increase temporarily by a factor up to ~30. The final span does depend on the operating conditions, fixed-flow conditions leading to a narrower span. It does not depend significantly on the value of that total flow, a fixed flow twice as high as the base case leading to a similar final span. The same is true for a head fixed twice as high as in the base case. It does not depend on how impermeable the aggregate is, provided the pseudoviscosity of water in the aggregate is orders of magnitude higher than that of water. Indeed, final channel porosities and aggregate shapes are similar under these conditions. The maximum temporary span, however, depends on the operating conditions. It is twice as high under twice as high fixed flow, power, or head conditions. This is rather unexpected and may be fortuitous. This means that the narrowest channel has time to become twice as clogged under these conditions before growth significantly slows down. However, the velocity span would eventually converge to the initial velocity span as the system fills up with biomass. In practice, a complete filling up is to be avoided as the resulting network conductivity would be orders of magnitude lesser than the initial one. It is also unlikely because an in situ bioremediation operator would likely use techniques to recover hydraulic conductivity before that happens.

If a sterile narrow bypass, 50 μm wide, is added in parallel to the system, it channels 1% of the total flow at $t = 0$. However, under fixed-flow conditions the bypass channels 92% of flow after 42 hours, while the widest-channel velocity is reduced by a factor of 13. This reduction is in sharp contrast to the minuscule 4% reduction of flow in the widest channel in the absence of a bypass (Figure 11). The flow reduction is despite the fact that by diverting flow from the seeded portion of the network, less substrate is available for growth, and clogging is reduced (Table 3). No breakthrough of substrate occurs through the seeded portion, indicating that biomass growth is limited by substrate supply.

To study the effect of initial seeding, each channel is replaced by a series of three identical channels. This will be called the "triple channel" network. The channels are now 1800 μm long and contain three colonies. Table 4 shows the conductivity decrease of each individual subchannel. Most of clogging occurs in the upgradient channels. The final network conductivity decrease is less than for the base case. Indeed, the downgradient channels must grow on substrate not degraded by the upgradient channels. As time passes, less substrate is

Table 3. Effect of Operating Conditions on the Average Velocity Span and Network Conductivity Decrease With Initial Velocity Span of 16

	Boundary Conditions: Fixed	Maximum Velocity Span	Final Velocity Span	Network Conductivity Decrease $k_0/k(k'_0/k')$[a]	End Time
Base Case	head	110	9.8	66	50
	power	140	4.6	620	50
	flow	210	5.6	1400	43.8
Water pseudoviscosity in aggregate 1000	head	100	8.3	55	50
	power	130	4.8	340	50
	flow	160	6	660	43.6
Water pseudoviscosity in aggregate 10	head	20	8	6.5	42.8
	power	26	9	6.8	41.4
	flow	27	14	5	36.4
Initial velocity twice as high as base case	head	230	8.7	130	50
	power	350	4.2	860	50
	flow	430	6.7	1270	42.6
Three channels in series	head	130	12	54	50
	power	170	4.2	270	50
	flow	190	3	780	43.2
One sterile 50 μm bypass	head	110	9.8	66 (41)	50
	power	140	3.6	270 (81)	50
	flow	180	4.1	370 (93)	46.2

[a]Here k is the seeded portion of the network conductivity decrease; k' is that of the whole network, including the sterile bypass, if applicable.

left, and downgradient growth stops. The relatively open downgradient channels signify that the network conductivity does not drop as much. Under fixed head or fixed power the upgradient channels in the "triple channel" network are more clogged than the respective analog channels in the base case as a higher flow rate (due to a lesser overall conductivity decrease of the triple channels with respect to the channels in the base case) results in more substrate being supplied and hence more growth occurring.

3.2. Periodic Network

To further study how distance from the supply source affects growth, we use an hexagonal lattice periodic network. Substrate flows from left to right, and the network is infinitely wide and thus periodic in that direction. Each 50 μm wide horizontal channel connects to two 100 μm wide oblique channels, resulting in the average velocity in the 50 μm wide channels being 4 times higher than in the 100 μm wide channels. The unit cell consists of three channels, as shown in Figure 12. We used a network with 6.5 cell repetitions in the direction along regional flow, that is, a total of seven 50 μm channels and six 100 μm wide channels.

For this case we supply 4 times more oxygen than phenol (when concentrations are normalized by K_S): Oxygen is in excess and can be used for cell decay when phenol is completely depleted. The hexagonal periodical network was operated with a fixed head across the network of 2.95×10^{-4} m. The resulting initial velocity in the 50 μm wide channels was 4 times higher than that in the 50 μm wide channel in the base case.

Figure 13 shows the effluent concentration of each channel as a function of time under fixed-head conditions. Because the channels are in series, these concentrations decrease from

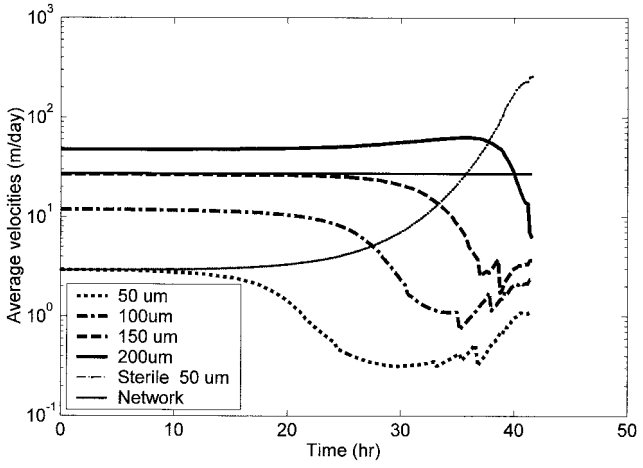

Figure 11. Average velocity in each channel of a network consisting of four different parallel channels and a sterile bypass. The average discharge across the network is 30 m d^{-1}.

Table 4. Conductivity Decrease of Each Channel Unit When Three Identical Channels (1–3) Are Linked in Series and Four Different Series Are Operated in Parallel

	Channel	Fixed Head	Fixed Power	Fixed Flow
Channel width, μm				
50	1[a]	110	280	560
	2	2.2	2.3	11
	3	1.6	1.6	2.7
100	1	130	540	1130
	2	4.2	5.4	68
	3	2.7	3.1	9.5
150	1	180	830	1510
	2	6.7	13.4	610
	3	4	6.5	47
200	1	210	1050	1280
	2	10.6	42.1	1070
	3	5.8	17.3	80
Network		67	306	780
Network base case		75	660	1360

[a]Channels 1 are upgradient.

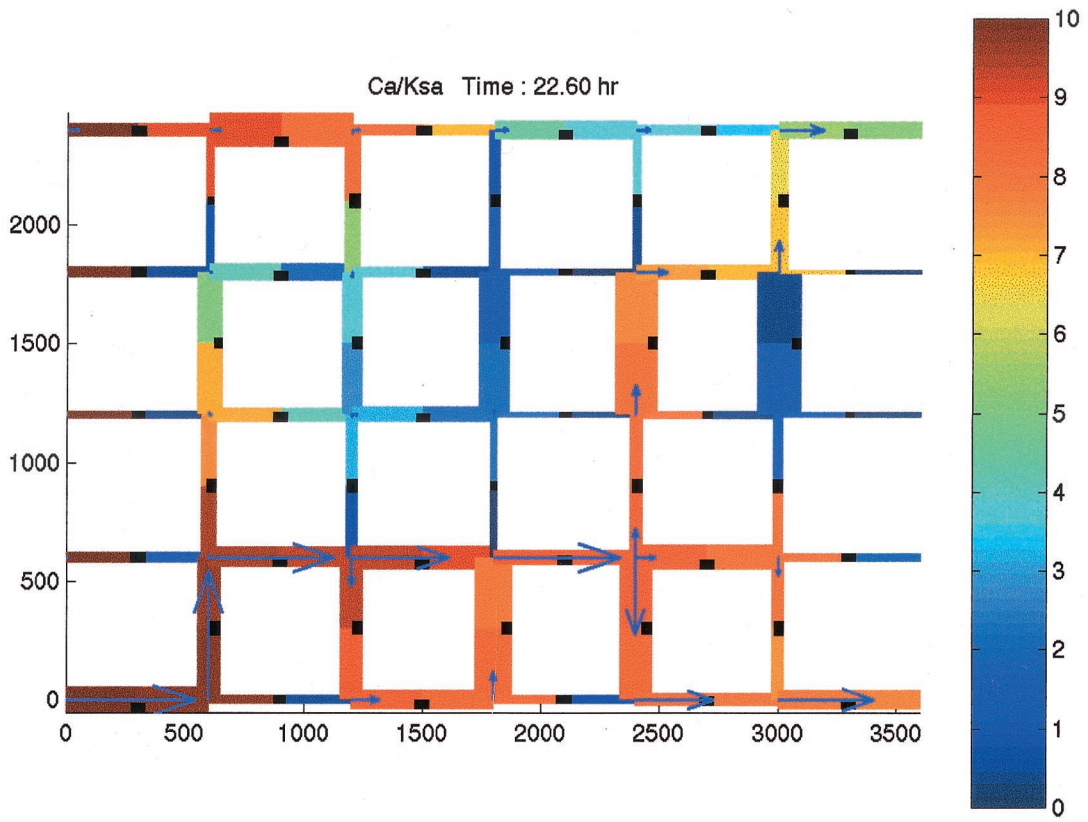

Plate 1. Flow path and concentration patterns in a random width square lattice network.

channel to channel, so that the highest concentration corresponds to the most upgradient channel and the lowest concentration corresponds to the most downgradient channel (network effluent). As time passes, most of the phenol is degraded in the upgradient channels, and the downgradient aggregates starve similarly to the triple channel network case. Owing to oxygen availability, downgradient aggregates decay, as is shown by oxygen consumption in all the channels. The sudden decrease in oxygen concentration around $t = 22$ hours occurs because the network clogs, the average velocity drops, and substrate supply sharply decreases.

Whereas conductivity keeps on decreasing in the most upstream channel, conductivity is slowly recovered downgradient. The average biomass decay rate is 0.087 day^{-1} in the most downgradient channel under fixed-flow conditions. This represents a 3% volume decrease in 9 hours. During the same time, growth is exponential in the first channel; its aggregate volume is increased by 440%. Thus most clogging results from plugging of upgradient channels, and downgradient porosity recovery is, in general, very small. Because the porosity-permeability decrease relation is highly nonlinear (see section 4), permeability recovery may occur by up to 30% for an aggregate volume decrease by 3%. This occurs for channels almost completely occluded by aggregates. A slight increase in the width of the

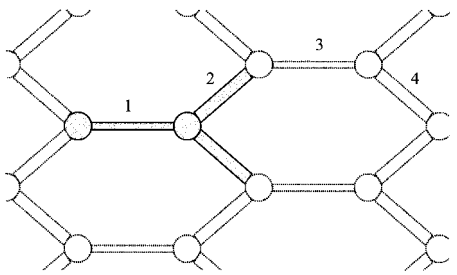

Figure 12. Hexagonal periodical network. The unit cell is indicated by solid lines. The dotted lines represent the repetitions. The nodes are schematically represented with circles.

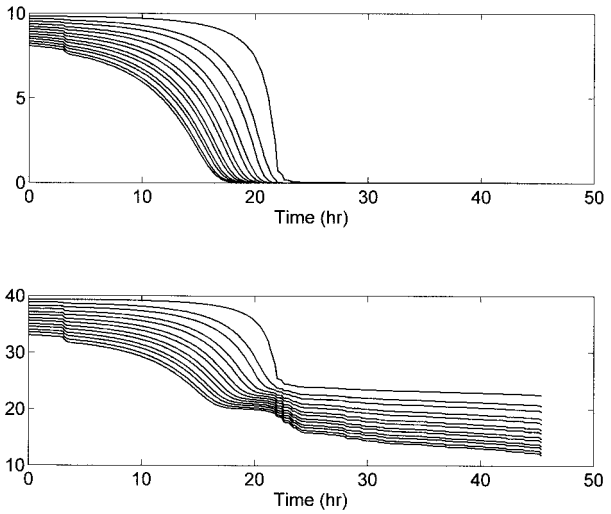

Figure 13. Effluent concentration for the hexagonal periodical network: (top) electron donor concentration at outlet, C_D/K_{sD}, and (bottom) electron acceptor concentration at outlet, C_A/K_{sA}.

open conduit has a high impact on permeability recovery. The network conductivity decreased by a factor of 340 under fixed flow, whereas several upgradient channels were filled with biomass (conductivity decrease of those channels by a factor of 1500–1800). This compares to a network conductivity decrease by a factor of 150 under fixed-power conditions and a factor of 50 under fixed-head conditions.

3.3. Square Lattice Networks

To better mimic real systems, 5×5 square lattice networks were investigated. In such networks a 5×5 square grid of nodes is connected by channels of the same length resulting in 50 channels. The channel widths were randomly drawn from a lognormal distribution (mean 123 μm, standard deviation 204 μm, and accepting widths only between 20 and 200 μm). Because of the small number of channels, channel width histograms of some realizations differed too much from the histogram of the parent distribution and such realizations were discarded. An acceptable realization is shown on Plate 1.

Plate 1 further shows flux, concentration, and biomass volume as follows. Arrows are proportional to the total flux through a channel. When an arrow is as long as a channel, all the flux through the network is flowing through that channel. To simplify biomass representation, colonies are represented with a rectangle of the same height of the actual colony and same area of the actual colony. One can then easily see when an aggregate occludes a channel. To simplify concentration representation, the upgradient half of a channel shows the influent concentration C_{supply}, and the downgradient half shows the effluent concentration. One can then see the effect of mixing in the nodes and consumption by aggregates within the channels.

Because of the two-dimensional structure, preferential flow paths, i.e., paths generally linking the widest channels, develop, as seen on the lower part of the network on Plate 1. Nevertheless, the overall behavior was similar to that described in sections 3.1 and 3.2 for simple systems. That is, the narrowest channels clog first; network conductivity is controlled by that of the preferential flow paths; growth occurs initially with similar growth rates throughout the network, then occurs mainly on the upgradient end of the network and in the preferential flow paths, resulting in greater permeability reductions there. Because of the dynamics of permeability decrease, fluid directions are reversed in some channels with time, average velocities fluctuate significantly, the preferential flow paths are modified, and local concentrations fluctuate widely.

4. Discussion

Because even small aggregates can occlude flow channels, the dynamics of aggregate-based models differ from the dynamics of biofilm-based models in terms of clogging and substrate consumption. In the variety of cases that we present, characteristic times of the 0.6 mm to 7.8 mm long systems, be it for growth, substrate consumption, or clogging, are, in general, shorter than 2 days. Experimentally, filamentous growth filled a significant portion of a 13.5×28 mm micromodel in 4 days [*Dupin and McCarty*, 1999], and clogging occurred after ~15 days in similar micromodels with other types of biological growth, mainly biofilm and aggregates [*Dupin and McCarty*, 2000]. In experiments reported by others, clogging characteristic times varied between 2 and 8 days depending on the size of the grains for mixed cultures [*Cunningham et al*., 1991] and varied on the order of 6 days for aggregate-forming microorganisms [*Vandevivere and Baveye*, 1992b] to 20 days [*Vandevivere and Baveye*, 1992a] for other microorganisms. Our simulations further show that from the moment a drop of concentration or permeability is detected to the moment complete plugging occurs, very little time passes (Figures 5 and 6). Thus control of a bioremediation process by feedback solely from these variables might be hard to achieve.

Our model shows that clogging occurs closer to the injection well, which tends to increase as time passes. This phenomenon has been observed in laboratory experiments [*Cunningham et al*., 1991; *Dupin and McCarty*, 1999, 2000; *Vandevivere and Baveye*, 1992a, 1992b] and in field studies [*Vecchioli et al*., 1980]. Clogging closer to the injection well could lead to permeability reduction that may be underestimated if the high heterogeneity of clogging is not properly taken into account (Table 4). Even if oxygen is in excess, downgradient permeability is unlikely to be recovered from biomass decay, as it is a very slow process compared to growth. Permeability is therefore more likely to be recovered by sloughing or predation by higher organisms, processes not considered in our simulations.

When bypasses are available, significant channeling has been observed through the more conductive ones. Thus once clogging is initiated, most flow should pass through sterile portions of the porous media or portions where biomass cannot attach because of high fluid velocities. In particular, when considering in situ bioremediation, proper sealing of the well casing to the formation is needed to avoid such channeling of flow.

Under fixed-flow conditions, intermittent substrate breakthrough occurs in the narrower pores. If we had placed the monitoring point at the outlet of the narrowest pores, we would have observed a very different signal than the network average concentration, approximated by the effluent concentration of the preferential flow paths. Thus part of the concentration fluctuations observed in field measurements might be caused by rerouting of flow and mass transport from clogged to less clogged areas.

As noted by *Cunningham et al*. [1991], who assumed a continuous biofilm, growth is initially exponential and identical in all the pores regardless of size. Growth eventually levels off when substrate becomes limiting, and this occurs at different times depending on the size of the channels. During substrate breakthrough, growth resumes and again becomes exponential.

In our square lattice network simulations, transport properties (permeability and substrate concentration) are controlled by clogging of preferential flow paths. The network conductivity is most affected by the clogging of the narrowest channels that form part of the preferential flow paths. Thus clogging in square lattice networks occurs before the widest pores clog but after the narrowest pores clog. *Torbati et al*. [1986] showed that the widest pores clogged more than the narrowest, with less variability in pore sizes after clogging. In our model the narrowest pores clog faster, but eventually, the conductivity of the widest pores decreases more. As a result, the range between the widest pore and the narrowest pore average velocities is reduced, for example, by a factor of 2–6 in parallel channel networks, consistent with the conclusion of *Torbati et al*. [1986]. However, they proposed that bigger pores would clog more because they see more substrate. Our model shows that the narrowest pores clog first, even though much less substrate may pass through them, because it takes less substrate to clog them. As a result, heterogeneity in the average velocities can increase temporarily by a factor of 20. The wider pores need

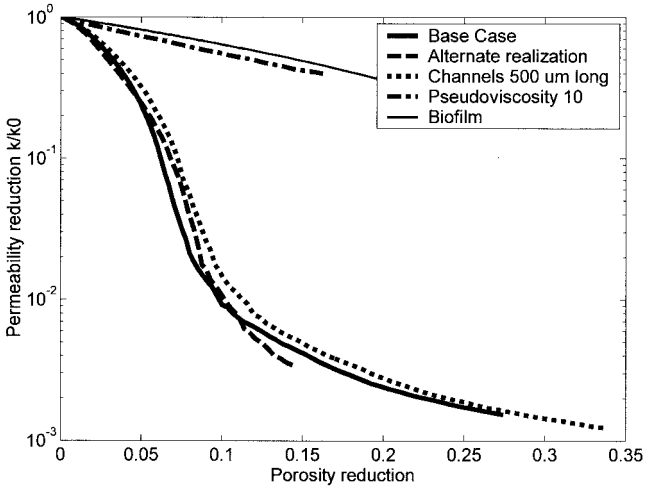

Figure 14. Relative hydraulic conductivity $k(t)/k(t = 0)$ as a function of porosity reduction for different network realizations and different parameter values.

more biomass to clog them, but they tend to receive more substrate and over longer periods and thus usually end up more clogged than the narrower channels. Heterogeneity is thus eventually reduced.

Taylor and Jaffe [1990a], *Taylor et al.* [1990], and *Vandevivere and Baveye* [1992b] have proposed the use of engineering curves relating porosity to permeability. Figure 14 shows such curves obtained from square lattice network simulations for different network realizations and different parameter values. In the base case, channels are 600 μm long, and pseudoviscosity is 2000 in the aggregates. The curves result from actual network simulations of aggregate clogging. However, the biofilm curve is achieved by redistributing as an impermeable layer on the pore walls the volume of the aggregates computed in the base case. Permeability decrease due to aggregate growth is more pronounced than that predicted by biofilm-based models for the same porosity reduction. This overall behavior has been indicated by *Vandevivere et al.* [1995], who noted that aggregate clogging better approaches observations than biofilm clogging. The explanation is that an aggregate can occlude a pore without filling it, while a continuous biofilm must completely fill it [*Rittmann*, 1993; *Vandevivere et al.*, 1995]. Porosity-permeability curves for different random realizations are quite similar. As expected, these curves do depend on the channel length, as it affects void volume hence porosity; when permeability is plotted as a function of aggregate volume, the curves are practically identical when modeling a given network realization with different channel lengths.

When the pseudoviscosity in the aggregate is set to 1000 times less than the water viscosity, there is no significant change in the porosity-permeability relation. When this pseudoviscosity is set to 10, the initial decrease change in the porosity-permeability relation is less steep, and in the case of square lattice networks it approaches the decrease expected in biofilm-based models (Figure 14).

As expected, porosity-permeability relations vary at the pore level (Figure 15). Small aggregates can fill narrow channels, while only wide aggregates can clog wide pores. This translates into a larger amount of biomass needed to clog large channels, and, because the aggregate area is about proportional to the square of the aggregate size in our simulations, a larger decrease in porosity if channels have the same length. The permeability decrease is steep while aggregates grow to reach the opposite wall of the channel: Under fixed flow, porosity is reduced by 12%, 25%, 37%, and 49% for, in that order, the 50, 100, 150, and 200 μm wide channels, while the pore permeability is reduced by a factor >100. Once aggregates have blocked a pore, the permeability does not decrease much as biomass increases.

Under fixed-head conditions, permeability decreases slightly less than under fixed-flow conditions for the same porosity decrease. Indeed, under fixed-flow conditions, nutrients are forced into the aggregates after clogging, and growth occurs throughout the aggregates, resulting in almost isotropic expansion. Under fixed-head conditions and close to clogging, aggregates are substrate-limited. Growth occurs then in the most upgradient portion of aggregates; that is, growth results in aggregate expansion along the axis of the channel, keeping channels open longer. Thus the porosity-permeability relation depends upon the operating conditions. Fixed flow leads to higher permeability decrease than fixed head for the same porosity decrease. Further modeling and experimental work is needed to validate this observation.

As a final remark, it is likely that biofilms consume more substrate than aggregates do for the same amount of biomass. Aggregates are compact, and the ratio of the surface available for external mass transfer to the volume of biomass is lower for aggregates than for a thin biofilm layer. That is, the center of a big aggregate may be nutrient-limited because of mass transfer limitations, while no part of a thin biofilm of the same mass would be starving. As a corollary, greater substrate removal is likely for the same permeability decrease if the porous media grains are covered by biofilms rather than by aggregates. From an engineering perspective, high substrate removal is desired, as it generally translates into high pollutant removal, but clogging is to be avoided. Thus when considering bioaugmentation, it is likely that biofilm-forming microorganisms should be preferred, as they would reduce operating costs related to clogging as shown in the simulations and increase efficiency of substrate uptake as further suggested here.

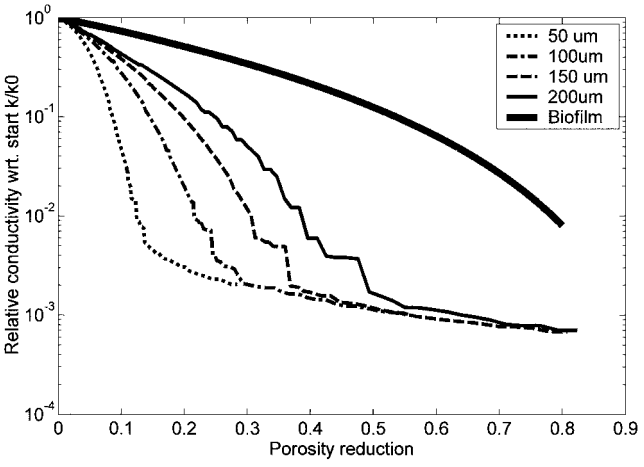

Figure 15. Permeability reduction versus porosity reduction under fixed-flow conditions for the different channels of the parallel channel network.

5. Model Limitations and Further Research

In this model we assume that fluid flow does not act upon the aggregates. If aggregates were to bend with the flow, the porosity-permeability decrease relation might be modified: A similar porosity reduction would induce a smaller permeability reduction as a flow path between an aggregate and an opposing wall would likely be kept open longer. However, to perform such a study, one would need to know some basic aggregate rheology, which must be obtained experimentally [*Dupin et al*., this issue].

The assumption $Pe_d \gg 1$ on the inlet and outlet boundaries of the aggregate is valid in most of our simulations. It is sometimes not valid at the end of a fixed-head operating scheme, but flux into the narrowest channels is negligible compared to that into the widest channels, so that nodal concentrations are not affected. However, average velocities used under fixed-head conditions are higher in our simulations than they are likely to be in the field, except perhaps very near a well injection.

As an alternative to nodal boundary conditions (21), (22), and (23) a gradient could be imposed at the outlet boundary of a channel, and more elaborate modeling of each node could be undertaken, yielding to alternative mixing hypotheses in each node and/or back diffusion from a node into a channel. For example, an alternative hypothesis to the nodal complete mixing is that no mixing occurs within a node: Concentrations follow along discrete stream tubes. This happens at sufficiently high velocities where diffusion is slow compared to advection but laminar flow still exists [*Berkowitz et al*., 1994]. Eventually, a model may be derived that takes into account nodal partial mixing. However, solving the network substrate transport problem would lead to network-wide iterations, as the channel boundary conditions would include upgradient information (as is the case in this paper) and downgradient information. Computations are likely to be lengthy. Given that our assumptions are valid most of the time in our simulations, such complexity does not appear necessary.

This model leads to the conclusion that aggregates cause greater conductivity decrease than biofilms. As suggested, biofilms are likely to consume more substrate than aggregates for a given permeability reduction. It has been observed [*Dupin and McCarty*, 2000] that biofilm and aggregates develop simultaneously from mixed culture. Filamentous growth has also been observed under acidic conditions [*Dupin and McCarty*, 1999]. That is, these morphologies are likely to coexist as a consequence of substrate injection in an aquifer. It would therefore be useful to study the combined effect of these growth morphologies, both on substrate consumption and on permeability reduction.

Finally, further research could include upscaling of this model. While direct finite element computations of each channel and node might not be feasible, engineering fitted curves might provide the simplification needed.

Acknowledgments. This research was supported in part by the Office of Research and Development, U.S. Environmental Protection Agency, through the Western Region Hazardous Substance Research Center under agreement R-815738, and in part by Elf Aquitaine, Inc. Additional support has been provided by NSF EAR-9523922 "Constitutive relations of solute transport and transformation." This article has not been reviewed by those organizations, and thus no official endorsement should be inferred.

References

Berkowitz, B., and R. P. Ewing, Percolation theory and network modeling applications in soil physics, *Surv. Geophys*., *19*(1), 23–72, 1998.

Berkowitz, B., C. Naumann, and L. Smith, Mass transfer at fracture intersections: An evaluation of mixing models, *Water Resour. Res*., *30*(6), 1765–1773, 1994.

Blunt, M., Effects of heterogeneity and wetting on relative permeability using pore level modelling, *SPE J*., *2*(3), 70–87, 1997.

Chen, B., A. Cunningham, R. Ewing, R. Peralta, and E. Visser, Two-dimensional modeling of microscale transport and biotransformation in porous media, *Numer. Methods Partial Differ. Eq*., *10*(1), 65–83, 1994.

Clement, T. P., B. S. Hooker, and R. S. Skeen, Macroscopic models for predicting changes in saturated porous media properties caused by microbial growth, *Ground Water*, *34*(5), 934–942, 1996.

Cunningham, A. B., W. G. Characklis, F. Abedeen, and D. Crawford, Influence of biofilm accumulation on porous media hydrodynamics, *Environ. Sci. Technol*., *25*(7), 1305–1311, 1991.

Dupin, H. J., Biological and hydrodynamic factors affecting aquifer clogging during in-situ bioremediation, Ph.D. thesis, Stanford Univ., Stanford, Calif., 1999.

Dupin, H., and P. McCarty, Mesoscale and microscale observations of biological growth in a silicon pore imaging element, *Environ. Sci. Technol*., *33*(8), 1230–1236, 1999.

Dupin, H., and P. L. McCarty, Impact of colony morphologies and disinfection on biological clogging in porous media, *Environ. Sci. Technol*., *34*(8), 1513–1520, 2000.

Dupin, H., P. Kitanidis, and P. L. McCarty, Pore-scale modeling of biological clogging due to aggregate expansion: A material mechanics approach, *Water Resour. Res.*, this issue.

Fatt, I., The network model of porous media, I, Capillary pressure characteristics, *Trans. Am. Inst. Min. Metall. Pet. Eng*., *207*, 144–159, 1956a.

Fatt, I., The network model of porous media, II, Dynamic properties of a single size tube network, *Trans. Am. Inst. Min. Metall. Pet. Eng*., *207*, 160–163, 1956b.

Fatt, I., The network model of porous media, III, Dynamic properties of networks with tube radius distribution, *Trans. Am. Inst. Min. Metall. Pet. Eng*., *207*, 164–181, 1956c.

Koplik, J., On the effective medium theory of random linear networks, *J. Phys. C Solid State Phys*., *14*, 4821–4837, 1981.

Laroche-Jaffrennou, C., O. Vizika, and F. Kalaydjian, Wettability heterogeneities in gas injection: Experiments and modelling, *J. Pet. Geosci*., *5*, 65–69, 1999.

McCarty, P. L., M. N. Goltz, G. D. Hopkins, M. E. Dolan, J. P. Allan, B. T. Kawakami, and T. J. Carrothers, Full-scale evaluation of in situ cometabolic degradation of richloroethylene in groundwater through toluene injection, *Environ. Sci. Technol*., *32*(1), 88–100, 1998.

Miller, C. T., A. J. Rabideau, and A. S. Mayer, Groundwater, *Res. J. Water Pollut. Control Fed*., *63*(4), 552–593, 1991.

Molz, F. J., M. A. Widdowson, and L. D. Benefield, Simulation of microbial growth dynamics coupled to nutrient and oxygen transport in porous media, *Water Resour. Res*., *22*(8), 1207–1216, 1986.

Paulsen, J. E., E. Oppen, and R. Bakke, Biofilm morphology in porous media, a study with microscopic and image techniques, *Water Sci. Technol*., *36*(1), 1–9, 1997.

Rittmann, B. E., The significance of biofilms in porous media, *Water Resour. Res*., *29*(7), 2195–2198, 1993.

Suchomel, B. J., B. M. Chen, and M. B. Allen, Macroscale properties of porous media from a network model of biofilm processes, *Transp. Porous Media*, *31*(1), 39–66, 1998a.

Suchomel, B. J., B. M. Chen, and M. B. Allen III, Network model of flow, transport and biofilm effects in porous media, *Transp. Porous Media*, *30*(1), 1–23, 1998b.

Taylor, S. W., and P. R. Jaffe, Biofilm growth and the related changes in the physical properties of a porous medium, 1, Experimental investigation, *Water Resour. Res*., *26*(9), 2153–2159, 1990a.

Taylor, S. W., and P. R. Jaffe, Substrate and biomass transport in a porous medium, *Water Resour. Res*., *26*(9), 2181–2194, 1990b.

Taylor, S. W., and P. R. Jaffe, Enhanced in-situ biodegradation and aquifer permeability reduction, *J. Environ. Eng*., *117*(1), 25–46, 1991.

Taylor, S. W., P. C. D. Milly, and P. R. Jaffe, Biofilm growth and the related changes in the physical properties of a porous medium, 2, Permeability, *Water Resour. Res*., *26*(9), 2161–2169, 1990.

Torbati, H. M., R. A. Raiders, E. C. Donaldson, M. J. McInerney, G. E. Jenneman, and R. M. Knapp, Effect of microbial growth on pore entrance size distribution in sandstone cores, *J. Ind. Microbiol*., *1*(4), 227–234, 1986.

Vandevivere, P., and P. Baveye, Effect of bacterial extracellular polymers on the saturated hydraulic conductivity of sand columns, *Appl. Environ. Microbiol*., *58*(5), 1690–1698, 1992a.

Vandevivere, P., and P. Baveye, Saturated hydraulic conductivity reduction caused by aerobic bacteria in sand columns, *Soil Sci. Soc. Am. J*., *56*(1), 1–13, 1992b.

Vandevivere, P., P. Baveye, D. Sanchez de Lozada, and P. DeLeo, Microbial clogging of saturated soils and aquifer materials: Evaluation of mathematical models, *Water Resour. Res*., *31*(9), 2173–2180, 1995.

Vecchioli, J., H. F. H. Ku, and D. J. Sulam, Hydraulic effects of recharging the Magothy aquifer, Bay Park, New York, with tertiary-treated sewage, *U.S. Geol. Surv. Prof. Pap*., *751-F*, 1980.

Wanner, O., A. B. Cunningham, and R. Lundman, Modeling biofilm accumulation and mass transport in a porous medium under high substrate loading, *Biotechnol. Bioeng*., *47*(6), 703–712, 1995.

Widdowson, M. A., Comment on "An evaluation of mathematical models of the transport of biologically reacting solutes in saturated soils and aquifers" by Philippe Baveye and Albert Valocchi, *Water Resour. Res*., *27*(6), 1375–1378, 1991.

H. J. Dupin, Geosciences Department, Exploration-Production Division, Gaz de France, 361 Avenue du Président Wilson BP 33, 93211 Saint-Denis-La-Plaine Cedex, France. (hubert.dupin@gazdefrance.com)

P. K. Kitanidis and P. L. McCarty, Department of Civil Engineering, Stanford University, Panama Mall and Samuel Morris Way, Stanford, CA 94305-4020. (kitanidis@ce.stanford.edu; mccarty@cive.stanford.edu)

(Received April 10, 2000; revised March 21, 2001;
accepted June 20, 2001.)